An Improved Scattering-Array-Based Decorrelation Technique for Enhanced MIMO Capacity in Realistic Multipath Scenarios

Simin Song, Chongwen Huang, *Member, IEEE*, Wei E. I. Sha, *Senior Member, IEEE*, and Xiaoming Chen, *Senior Member, IEEE*

***Abstract*—An improved phase-correcting-element (PCE)-based decorrelation technique is proposed in this letter. Unlike prior approaches, the proposed PCE scheme explicitly models both amplitude attenuation and phase shift under oblique incidence, and leverages the QuaDRiGa stochastic channel model to capture practical channel characteristics. A 2×4 dual-polarized patch array with PCEs operating at 3.5 GHz is fabricated to validate the proposed decorrelation method. Simulations and measurements agree well, showing up to 36% improvement in channel capacity and 25% increase in effective degrees of freedom compared to conventional arrays without PCEs.**

***Index Terms*—Multiple-input–multiple-output (MIMO) array, scattering array, spatial correlation.**

I. Introduction

MULTIPLE-INPUT–multiple-output (MIMO) technology has become a fundamental technique to enhance channel capacity and spectral efficiency [1]. Traditionally, increasing the array aperture size and channel numbers are straightforward methods to enhance MIMO capacity [2]. However, for aperture-constrained MIMO arrays, it is difficult to further increase array gains [3], and further MIMO performance improvement must rely on decorrelating closely spaced antenna elements without significant distortion of their radiation patterns. In typical base station (BS) deployments, horizontal interelement spacing is about $0.5\lambda_0$ (where λ_0 is the free-space wavelength). Nonetheless, due to the limited angular spread at the BS side, even half-wavelength spaced elements can exhibit high correlation, which directly limits spatial correlation and MIMO capacity [4].

Numerous approaches have been proposed to reduce correlation by decreasing mutual coupling between array elements, such as decoupling grounds [5], [6], metamaterials [7], [8], defected ground structure (DGS) [9], [10], electromagnetic bandgap (EBG) designs [11], and other methods [12], [13], [14], [15]. However, reducing mutual coupling does not always guarantee correlation reduction, especially in real-life nonuniform multipath environments [4]. An effective decorrelation technique requires modifying the antenna radiation characteristics to match the angular power distributions.

Tilted beam techniques, such as placing frequency selective surfaces (FSSs) above array apertures [16], can reduce correlation at the cost of poor cellular coverage. Scatterer-array-based approaches [17], [18], [19] attempt to stretch the effective phase center distributions by modifying near-field phase distributions. Nevertheless, earlier works either assumed three-dimensional (3-D) uniform propagation environments or exhibited diminishing returns for large arrays, limiting their scalability and accuracy of multipath environment assessment.

The electromagnetic information theory provides a foundational framework that fully accounts for spatial correlation effects in modern wireless systems, enabling effective exploitation of spatial-temporal information characteristics [20]. On this basis, a programmable metasurface antenna is proposed to approach the theoretical upper limit of the information mapping efficiency [21].

A 3-D topology antenna array [22] is proposed for breaking the degree of freedom (DoF) limit of aperture-constrained 2-D antenna arrays, which reduces spatial correlation by expanding the equivalent projection area through vertical dimension exploitation. However, the benefits of 3-D arrays can only be realized in linear compact arrays less than $0.5\lambda_0$ with highly complex hardware.

To address these challenges, a phase-correcting-surface (PCS)-based near-field optimization technique [23] has been proposed for large-scale MIMO arrays, which reduces antenna correlations by optimizing the near-field phase distribution over the array aperture, thereby enhancing radiation pattern orthogonality without tilting main beams or sacrificing cellular coverage. However, this method makes several simplifications in the PCS design: it assumes each PCS element is lossless and only considers the phase shift caused by the normal incident wave; and an overly simple ray-tracing channel model is used in the optimization. These simplifications ignore oblique incidence effects and ultimately only achieve less than 10% capacity improvement in more realistic multipath channels.

In this work, an improved phase-correcting-element (PCE)-based decorrelation technique is proposed for MIMO performance enhancement. The proposed PCE model is different from the PCS presented in [23] in the following ways.

Received 11 May 2025; revised 24 June 2025; accepted 6 August 2025. Date of publication 11 August 2025; date of current version 8 October 2025. This work was supported by Key Research and Development Program of Shaanxi under Grant 2024GX-ZDCYL-01-26. *(Corresponding author: Xiaoming Chen.)*

Simin Song and Xiaoming Chen are with the School of Information and Communications Engineering, Xi'an Jiaotong University, Xi'an 710049, China (e-mail: xiaoming.chen@mail.xjtu.edu.cn).

Chongwen Huang and Wei E. I. Sha are with the College of Information Science and Electronic Engineering, Zhejiang University, Hangzhou 310027, China.

Digital Object Identifier 10.1109/LAWP.2025.3597644

1) It considers the complex-value transmission response of the PCE element under more common oblique incidence.
2) It considers a more realistic geometry-based stochastic channel mode.

II. Analysis and Design Examples

A. Correlation and Channel Capacity of Array Antenna

The spatial correlation between antenna elements in a MIMO array is a critical factor influencing system performance, particularly in real-life (nonisotropic) multipath environments. To address this, the correlation coefficient between two arbitrary antenna elements *m* and *n* can be rigorously defined using their embedded radiation patterns $\vec{E}_m(\Omega)$ and $\vec{E}_n(\Omega)$, incorporating both polarization components and propagation channel characteristics

$$\rho_{mn} = \frac{\oint G_{mn}(\Omega) d\Omega}{\sqrt{\oint G_{mm}(\Omega) d\Omega}\sqrt{\oint G_{nn}(\Omega) d\Omega}} \quad (1)$$

$$G_{mn}(\Omega) = \kappa E_{\theta m}(\Omega) E^*_{\theta n}(\Omega) P_\theta(\Omega) + E_{\phi m}(\Omega) E^*_{\phi n}(\Omega) P_\phi(\Omega) \quad (2)$$

$$\mathbf{R} = \frac{1}{N}\mathbb{E}\left[\mathbf{H}\mathbf{H}^H\right] \quad (3)$$

where $P_\theta(\Omega)$ and $P_\phi(\Omega)$ represent the power angular spectra (PAS) of elevation (θ) and azimuth (ϕ) polarized waves, respectively, *N* is the number of transmitting antennas, $\mathbb{E}$ denotes expectation, ρ_{mn} is an element in the correlation matrix $\mathbf{R}$, and κ denotes the cross-polarization discrimination (XPD). This formulation explicitly accounts for the joint effects of antenna radiation patterns and realistic propagation channels.

While correlation coefficients are suitable for small arrays, characterizing large-scale arrays requires a more concise metric. The DoF (or diversity measure) provides a scalar representation of the effective number of uncorrelated antennas [24]

$$\text{DoF} = \frac{\text{tr}(\mathbf{R})^2}{\text{tr}(\mathbf{R}^2)} \quad (4)$$

where $\mathbf{R}$ is the correlation matrix. The DoF ranges from 1 (fully correlated) to *N* (fully uncorrelated), offering a unified criterion to evaluate the overall array correlation performance.

The ultimate goal of MIMO array optimization is to maximize its channel capacity. For a given reference signal-to-noise-ratio (SNR) γ, the ergodic capacity can be expressed as [25]

$$C = \mathbb{E}\left\{\log_2 \det\left(\mathbf{I} + \frac{\gamma}{N}\mathbf{H}\mathbf{H}^H\right)\right\} \quad (5)$$

where $\mathbf{H}$ is the channel matrix, the superscript ^{H} is the Hermitian (conjugate transpose) operator, and $\mathbf{I}$ is an identity matrix. It is usually calculated based on simulated or measured channels.

B. Decorrelation Technique Analysis

Both power and correlation influence the MIMO capacity. While the phase patterns dominate the spatial correlation between array elements [17], amplitude patterns dominate the received power. Thus, reducing correlation while preserving good beam coverage is critical for MIMO performance enhancement. The previously proposed PCS-based decorrelation method modified the near-field phase distribution of an array antenna aperture to increase the orthogonality of its far-field patterns, thereby reducing interelement correlation [23]. Therein, two simplifications were adopted.

1) Each PCS element was treated as lossless, only imposing a phase shift with unity transmission magnitude.
2) Only normal-incidence phase shifts were considered, ignoring the angular dependence of oblique waves. These simplifications failed to capture oblique-incidence phase shifts, and transmission losses significantly altered the PCS response, diminishing the MIMO performance enhancement.

To address these limitations, our work introduces a more realistic model with two key enhancements.

1) More realistic PCE modeling: Each PCE is viewed as a two-port electromagnetic network characterized by a complex transmission coefficient that depends on incidence angles. Instead of a fixed-phase-shift element, the PCE unit is modeled with both amplitude attenuation and phase delay. The oblique-incidence near-field model is shown in Fig. 1(a). The incoming wave (denoted by the red arrow) from the BS antenna propagates through the PCE Sub6 and arrives at E-field sampling point E_i. Compared with free space propagation, the additional phase shift introduced at point E_i corresponds to the phase shift of Sub6 under θ_{inc}. The oblique-incidence transmission responses of the PCE are simulated in the CST unit cell condition.
2) More realistic propagation channel modeling: QuaDRiGa [26], a geometry-based stochastic channel model, is used in our proposed decorrelation framework instead of the simplified ray-tracing scattering model used in [23]. Unlike prior approaches that fix angular spreads or assume ideal flat fading, QuaDRiGa channel model dynamically produces multipath components with path loss, distance-dependent shadow fading, cluster angular spreads, and time evolution compliant with 3GPP standards [26]. This improvement captures the interplay between array antenna correlation and real-life propagation effects.

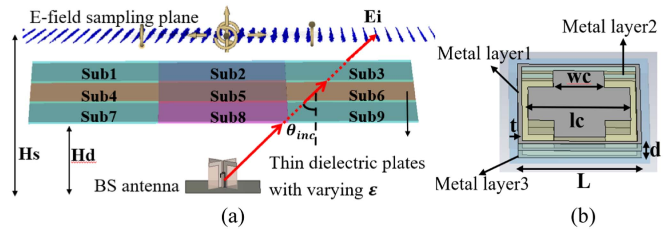

Fig. 1. (a) Oblique-incidence near-field channel model. (b) Configuration of the PCE unit. Hs = 102.8, Hd = 68.6, $L = 30$, t= 2, $d = 9$ and $wc = 0.5lc$ (unit: mm).

The improved decorrelation optimization algorithm is illustrated in the flowchart provided in Fig. 2. Here, the near-to-far-field conversion algorithm based on an orthogonal basis matrix in [23] is adopted. **b** is the electric-field sampling matrix, and ΔDoF is designed to be 0.15 in consideration of the tradeoff between increased DoF and realized MIMO capacity. We use the MATLAB surrogate optimization function for global optimization of the given problem. The total optimization process takes about 13 min (on a standard personal computer with Intel Core i7-9700 CPU and 32 GB RAM) and converges after 800 iterations.

PCE-based Decorrelation Optimization Algorithm

Iutput: Embedded far-field patterns $\vec{E}_{iwo}(\theta,\phi)$ without PCE, $i = 1,\ldots,N$.
Import $\vec{E}_{iwo}(\theta,\phi)$ into QuaDRiGa channel to generate channel matrix H_{wo}.
Calculate baseline MIMO capacity C_{wo} and diversity DoF_{wo}.
Extract near-field E-field sampling coefficients $\mathbf{b}_{iwo}$ for each antenna element, $i = 1,\ldots,N$.
Initialize PCE configuration as a new N-dimentional vector.
while objective not satisfied **do**
  Calculate near-field E-field coefficients
  $\mathbf{b}_{iwi} = \mathbf{b}_{iwo} \cdot |T_i(\theta,\phi)|\, e^{j\varphi_i(\theta,\phi)}$, $i = 1,\ldots,N$.
  Calculate far-field patterns $\vec{E}_{iwi}(\theta,\phi) = \mathbf{b}_{iwi} \cdot \vec{e}$, $i = 1,\ldots,N$.
  Import $\vec{E}_{iwi}(\theta,\phi)$ into QuaDRiGa to generate channel matrix H_{wi}.
  Calculate updated MIMO capacity C_{wi} and diversity DoF_{wi}.
  Evaluate objective and check constraints:
  maximize $f(PCE) = C_{wi} - C_{wo}$;
  subject to $\mathrm{DoF}_{wi} - \mathrm{DoF}_{wo} > \Delta\mathrm{DoF}$, $f(PCE) > 0$.
  if not fullfill **then**
    Update PCE configuration.
  end if
end while
Output: Optimized PCE configuration.

Fig. 2. Flowchart of the decorrelation optimization algorithm for an N-ports MIMO array. The subscripts wi and wo denote with and without PCE, respectively. ΔDoF represents the required improvement in DoF that must be achieved to ensure decorrelation.

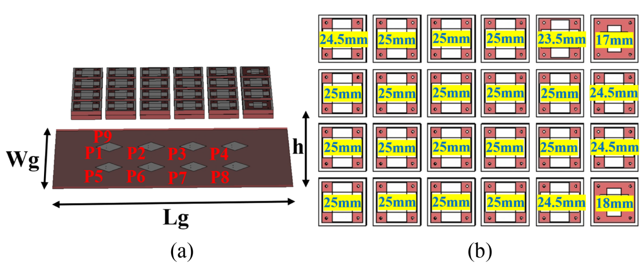

Fig. 3. 2×4 patch array with PCEs. (a) Perspective view and (b) corresponding length of metal cross lc. $Lg = 240$, $Wg = 170$, $h = 68.6$ (unit: mm).

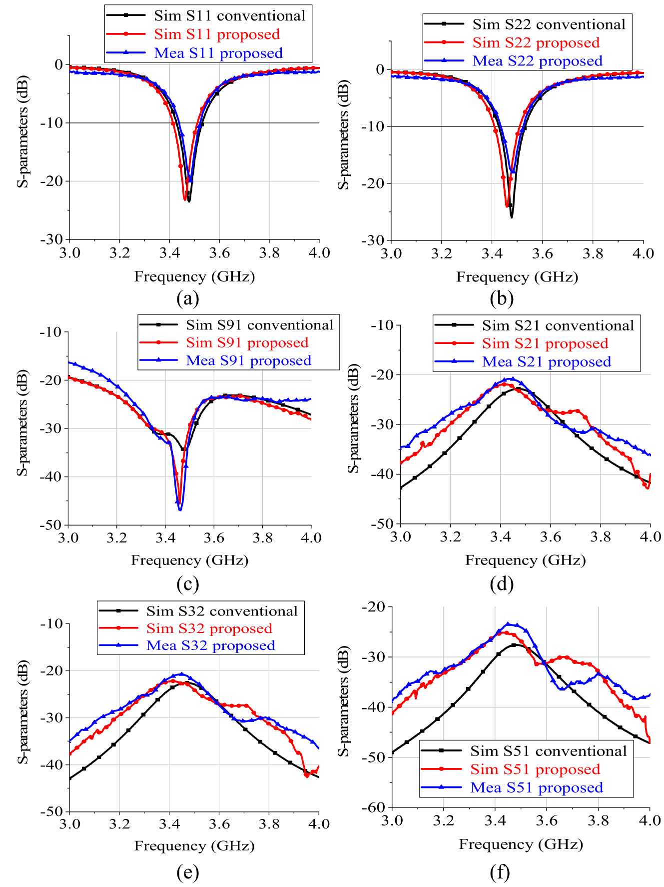

Fig. 4. Simulated and measured S-parameters of the 2×4 patch array with/without PCEs. (a) S_{11}, (b) S_{22}, (c) S_{91}, (d) S_{21}, (e) S_{32} and (f) S_{51}.

C. 2×4 Patch Array With PCEs

A $2 \times 4 \pm 45^\circ$ dual-polarized patch array operating at 3.5 GHz is designed to validate the proposed decorrelation optimization technique, as shown in Fig. 3. The interelement spacings of the patch array are $0.5\lambda_0$ in the horizontal direction and $0.7\lambda_0$ in the vertical direction. The patch array is printed on a 2 mm thick FR-4 substrate (with a relative permittivity of 4.3 and a loss tangent of 0.0025), and the port numbers are marked in Fig. 3(a), P1 to P8 correspond to $+45^\circ$ polarization ports.

The PCE array composed of three metallic layers and two dielectric layers (9 mm thick F4BM220 with 2.2 relative permittivity and 0.001 tangential loss) is positioned $0.8\lambda_0$ above the array aperture as a tradeoff between pattern maintenance and MIMO capacity improvement. The PCE unit, featuring a square metal ring and a cross-shaped structure [shown in Fig. 1(b)], dynamically adjusts transmission phase (-112° to 31°) and amplitude ($|T| > 0.77$) by varying the cross length (15 mm to 25 mm). To avoid degrading the array's impedance matching and radiation efficiency, we constrain the PCE configurations with $|T| > 0.8$. The final optimized PCE parameters are listed in Fig. 3(b).

To quantify the MIMO performance enhancement, the link-level validation of the PCE-assisted array is carried out with QuaDRiGa. The 2×4 BS array is deployed at a height of 25 m with a 7° downtilt, serving the target hexagonal cell of radius 167 m. User equipments (UEs) at 1.5 m height are randomly distributed within the target cell, moving at 1 m/s along random trajectories. 3GPP urban micro (UMi) model in the non-line-of- sight (NLOS) scenario is selected here. The embedded radiation patterns of the BS array with PCEs are imported into QuaDRiGa with 1000 time-samples to calculate the cumulative distribution function (CDF) of the sum capacity and DoF.

III. Experimental Validation

To validate the proposed decorrelation concept, a 2×4 prototype array has been designed, fabricated, and tested. The photograph of the prototype array is presented in Fig. 6(b). The prototype array is supported by several nylon columns (with a relative permittivity of 1.65) and a piece of foam (with a relative permittivity of 1.07). These support structures have little impact on the impedance bandwidth of the prototype antenna.

Fig. 4 shows the simulated and measured S-parameters of the patch array with and without PCEs. As can be seen, the measured results align well with the simulated ones. Moreover, the PCEs have minimal impacts on the array's matching and mutual coupling, with all coupling levels below -20 dB.

Fig. 5 illustrates the simulated and measured radiation patterns of the left two elements [Port1 and Port2 shown in Fig. 3(a)] at 3.5 GHz. As can be seen, the gains with PCEs are increased by roughly 1.5 dB to 1.9 dB with narrowed vertical beamwidths and enhanced cross-polarization discrimination (XPD) at broadside. Given that the elevation angular spread in realistic multipath

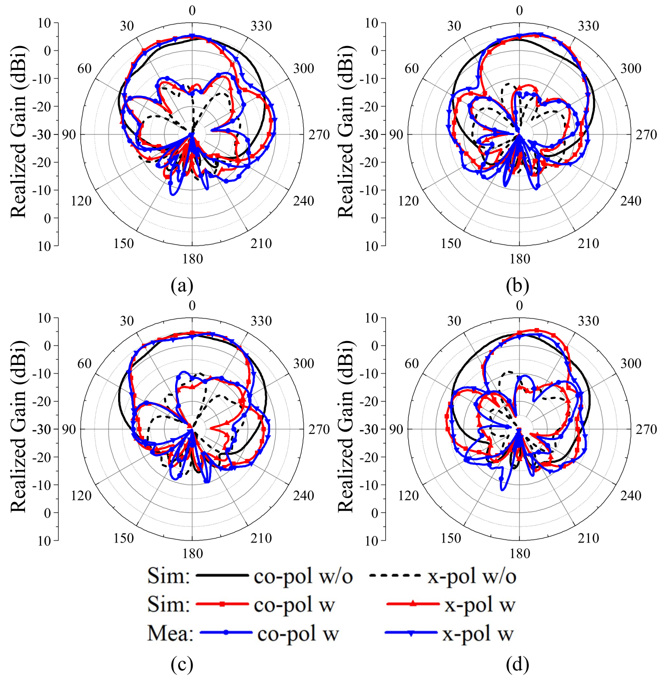

Fig. 5. Simulated and measured radiation patterns of the 2 × 4 patch array Port1 and Port2 with/without PCEs at 3.5 GHz in (a) and (c) H-plane (*xz*-plane) and (b) and (d) V-plane (*yz*-plane).

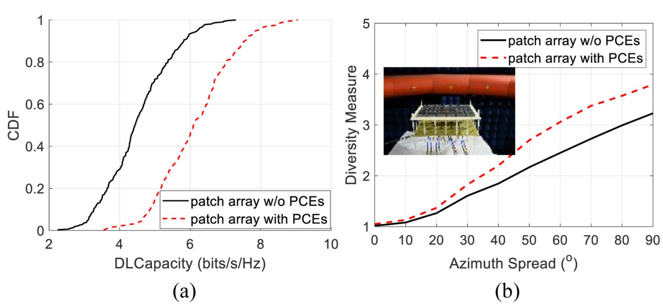

Fig. 6. MIMO performance enhancement. (a) CDF of the sum capacity and (b) diversity measure of the patch array with and without PCEs.

scenarios is narrower than the azimuth angular spread, the narrower vertical-plane beam scarcely undermines cellular coverage for BS applications and, instead, increases the received power and reduces interference. Thereby, the enhancement of MIMO channel capacity arises from two contributing factors: partially due to increased diversity measure (spatial multiplexing gain) and partially from gain improvement. Measurements agree well with simulations. Crucially, these benefits operate within a fundamental tradeoff: Larger array dimensions and wider element spacings inherently deliver higher baseline spatial diversity without decorrelation structures, consequently diminishing the optimization headroom for capacity enhancement through DoF exploitation.

Fig. 6 presents the MIMO performances of the patch array with PCEs. The DoF and the sum capacity of the patch array are improved by 25% and 36% on average, respectively. Loading PCE mainly improves DoF in the horizontal plane. The equivalent array element spacings are increased to $0.58\lambda_0$ and

TABLE I
COMPARISON WITH RELEVANT WORKS

Ref.	Array config.	Decorrelation method	Multipath scenario	Capacity/DoF enhancement
[16]	1×2	Tilting beam	Isotropic	N.A. (95% reduction in ρ)
[17]	1×4	Near-field phase adjustment	Non-isotropic	12.2%/10%
[18]	1×4	Stretching phase center distance	Non-isotropic	4%/5%
[22]	1× 9	3D-array	3D 3GPP UMa	7%/11%
[23]	1×4 2×8	Near-field optimization	WINNER+ UMi	8%/7% 10%/9%
This work	2×4	Near-field optimization	Non-isotropic	36%/25%

$0.93\lambda_0$ in the horizontal direction and vertical direction, respectively, leading to increased array aperture and MIMO capacity. Obviously, the proposed PCE-based decorrelation technique can effectively improve the BS MIMO performance, demonstrating a significant performance improvement over the previous works [17], [18], [19], [20], [21], [22], [23] (cf. Table I).

Existing decorrelation techniques face several critical limitations in practical deployments.

1) Beam tilting methods [16] sacrifice broadside radiation patterns essential for cellular coverage and cause strong mutual couplings.
2) Scatterer arrays [17], [18] achieve decorrelation without beam distortion but fail to expand to large MIMO arrays due to prohibitive manufacturing complexity and cost.
3) 3-D topology arrays [22] are only profitable for compact configurations ($\leq 0.5\lambda_0$), requiring sophisticated hardware design with substantial complexity and cost.
4) The PCS-based near-field optimization algorithm is suitable for large MIMO arrays, but the actual performance of this work is limited by the overly simplified model. The proposed PCE-based decorrelation method overcomes these limitations by preserving broadside radiation, adapting to oblique incidence with large MIMO architectures, and demonstrating a significant capacity and DoF improvements of 36% and 25%, respectively.

IV. CONCLUSION

This study presents a novel PCE-based decorrelation technique that significantly enhances MIMO capacity in realistic multipath scenarios. By modeling oblique-incidence transmission responses and integrating a QuaDRiGa channel framework, the proposed method effectively reduces spatial correlation while maintaining cellular coverage. Experimental validation using a 2 × 4 patch array with PCEs confirms a 36% capacity enhancement and a 25% DoF improvement, attributed to optimized near-field phase distributions and balanced eigenvalue profiles. This work bridges the gap between theoretical pattern synthesis and practical antenna design, offering a scalable solution for next-generation massive MIMO deployments in realistic multipath environments.

REFERENCES

[1] R. He, B. Ai, G. L. Stuber, G. Wang, and Z. Zhong, "Geometrical based modeling for millimeter wave MIMO mobile-to-mobile channels," *IEEE Trans. Veh. Technol.*, vol. 67, no. 4, pp. 2828–2863, Apr. 2018.

[2] C. A. Balanis, *Antenna Theory: Analysis and Design*. Hoboken, NJ, USA: Wiley, 2015.

[3] D. A. B. Miller, "Waves, modes, communications, and optics: A tutorial," *Adv. Opt. Photon.*, vol. 11, no. 3, pp. 679–825, 2019.

[4] X. Chen et al., "Revisit to mutual coupling effects on multi-antenna systems," *J. Commun. Inf. Netw.*, vol. 5, no. 4, pp. 411–422, Dec. 2020.

[5] S. Zhang, X. Chen, and G. F. Pedersen, "Mutual coupling suppression with decoupling ground for massive MIMO antenna arrays," *IEEE Trans. Veh. Technol.*, vol. 68, no. 8, pp. 7273–7282, Aug. 2019.

[6] S. Song, X. Chen, Y. Da, and A. Kishk, "Broadband dielectric resonator antenna array with enhancement of isolation and front-to-back ratio for MIMO application," *IEEE Antennas Wireless Propag. Lett.*, vol. 21, no. 7, pp. 1487–1491, Jul. 2022.

[7] Z. Wang et al., "A meta-surface antenna array decoupling (MAAD) method for mutual coupling reduction in a MIMO antenna system," *Sci. Rep.*, vol. 8, 2018, Art. no. 3152.

[8] J. Tang et al., "A metasurface superstrate for mutual coupling reduction of large antenna arrays," *IEEE Access*, vol. 8, pp. 126859–126867, 2020.

[9] L. Wang, Z. Xing, K. Wei, R. Xu, and J. Li, "S-shaped periodic defected ground structures to reduce microstrip antenna array mutual coupling," *Electron. Lett.*, vol. 52, no. 15, pp. 1288–1290, 2016.

[10] B. Qian, X. Chen, L. Zhao, J. Chen, and A. A. Kishk, "Reduced cross-polarization and backside radiations for rectangular microstrip antennas using defected ground structure combined with decoupling structure," *IEEE Antennas Wireless Propag. Lett.*, vol. 22, no. 3, pp. 517–521, Mar. 2023.

[11] E. Rajo-Iglesias, Ó. Quevedo-Teruel, and L. Inclan-Sanchez, "Mutual coupling reduction in patch antenna arrays by using a planar EBG structure and a multilayer dielectric substrate," *IEEE Trans. Antennas Propag.*, vol. 56, no. 6, pp. 1648–1655, Jun. 2008.

[12] K.-L. Wu, C. Wei, X. Mei, and Z.-Y. Zhang, "Array-antenna decoupling surface," *IEEE Trans. Antennas Propag.*, vol. 65, no. 12, pp. 6728–6738, Dec. 2017.

[13] L. Sun, Y. Li, Z. Zhang, and H. Wang, "Antenna decoupling by common and differential modes cancellation," *IEEE Trans. Antennas Propag.*, vol. 69, no. 2, pp. 672–682, Feb. 2021.

[14] H. Yang et al., "Aperture reduction using downward and upward bending arms for dual-polarized quadruple-folded-dipole antennas," *IEEE Antennas Wireless Propag. Lett.*, vol. 22, no. 3, pp. 645–649, Mar. 2023.

[15] T. Liu et al., "Compact U6G massive MIMO antenna arrays with double-layer partial reflective decoupling layers for mutual coupling suppression," *IEEE Open J. Antennas Propag.*, vol. 4, pp. 764–778, 2023.

[16] T. Hassan, M. U. Khan, H. Attia, and M. S. Sharawi, "An FSS based correlation reduction technique for MIMO antennas," *IEEE Trans. Antennas Propag.*, vol. 66, no. 9, pp. 4900–4905, Sep. 2018.

[17] M. Li, X. Chen, A. Zhang, A. A. Kishk, and W. Fan, "Reducing correlation in compact arrays by adjusting near-field phase distribution for MIMO applications," *IEEE Trans. Veh. Technol.*, vol. 70, no. 8, pp. 7885–7896, Aug. 2021.

[18] Y. Wang et al., "Improvement of diversity and capacity of MIMO system using scatterer array," *IEEE Trans. Antennas Propag.*, vol. 70, no. 1, pp. 789–794, Jan. 2022.

[19] Y. Wang, X. Huang, J. Zhao, Z. Zhong, W. E. I. Sha, and X. Chen, "Experimental investigation of scatterer-array-based decorrelation technique applied to real multiple-input multiple-output base station," *Electron. Lett.*, vol. 59, no. 8, Apr. 2023, Art. no. e12796.

[20] X. Bai, S. Tan, S. Mikki, E. Li, and T.-J. Cui, "Information-theoretic measures for reconfigurable metasurface-enabled direct digital modulation systems: An electromagnetic perspective," *Prog. Electromagn. Res.*, vol. 179, pp. 1–18, 2024.

[21] H. Wu et al., "A programmable metasurface antenna that approaches the wireless information mapping limit," *Nature Electron.*, vol. 9, pp. 179–191, 2025.

[22] S. S. A. Yuan et al., "Breaking the degrees-of-freedom limit of holographic MIMO communications: A 3-D antenna array topology," *IEEE Trans. Veh. Technol.*, vol. 73, no. 8, pp. 11276–11288, Aug. 2024.

[23] Y. Wang, X. Chen, H. Pei, W. Sha, Y. Huang, and A. Kishk, "MIMO performance enhancement of MIMO arrays using PCS-based near-field optimization technique," *Sci. China Inf. Sci.*, vol. 66, no. 6, Jun. 2023, Art. no. 162302.

[24] M. T. Ivrlac and J. A. Nossek, "Diversity and correlation in Rayleigh fading MIMO channels," in *Proc. IEEE 61st Veh. Technol. Conf.*, 2005, pp. 151–155.

[25] J. Paulraj, R. U. Nabar, and D. A. Gore, *Introduction to Space-TimeWireless Communications*. Cambridge, U.K.: Cambridge Univ. Press, 2003.

[26] S. Jaeckel et al., "QuaDRiGa: A 3-D multi-cell channel model with time evolution for enabling virtual field trials," *IEEE Trans. Antennas Propag.*, vol. 62, no. 6, pp. 3242–3256, Jun. 2014.